International Journal of Thin Films Science and Technology

http://dx.doi.org/10.18576/ijtfst/130207

Commercial Si Solar Cell Efficiency Improvement by Gamma Radiation, Plasma Treatment and Oxides Front Layer Depositions

Gh. A. Al-zaidi [1], H. A. Saudi [1], Ibrahim A. Nassar [2], M. S. Shalaby [3], and K. Sedeek [4,]*

[1] Physics Department, Faculty of Science, Al-Azhar University (Girls Branch), Cairo, Egypt
[2] Department of Electricity, Faculty of Engineering, Al-Azhar University, Cairo, Egypt
[3] Solid-State Physics and Accelerators Department, National Center for Radiation Research and Technology, Egypt
[4] Nano-Materials Lab, Physics Department, Faculty of Science, Al-Azhar University (Girls Branch), Cairo, Egypt

Received: 7 Feb. 2024, Revised: 15 Apr. 2024, Accepted: 27 Apr. 2024
Published online: 1 May 2024

Abstract: In this work the potential of atmospheric agents such as gamma rays and plasma on conventional solar cell efficiency has been followed. Improving the device performance by depositing a ZnO or $SrTiO_3$ layer on the front surface of both monocrystalline and polycrystalline Si cells has been also achieved. The electrical parameters detected by measuring the I-V characteristic are discussed. The results were analyzed using modified thermal emission theory to estimate the barrier height (B*o*), ideality factor (n), series and shunt resistances (R*s* and R*sh*). Gamma irradiation at 1 kGy increased V_{OC}, I*sc*, V_{mp}, and I*mp*, hence the maximum output power (P*m*) and efficiency (η) of both cell types. Concerning the dense plasma focus (DPF) effect, H2 gas flow was detected to increase the efficiency by 16.5% and 22.5%, respectively for monocrystalline and polycrystalline cells. The potential effect of the deposition of a thin layer of SrTiO3 (SrTiO3/Si) or ZnO (ZnO/Si) led to efficiency improvement of 24% and 23%, respectively for monocrystalline cells. The effect of light trapping and the reduction of recombination by the front layer on cell performance and the role played by grain boundaries of polycrystalline cells were discussed.

Keywords: Commercial Si solar cells, Gamma rays, Dense plasma focus, ZnO/Si and SrTiO3/Si multilayers.

1 Introduction

For the last few decades, silicon solar cells acted as a reasonable solution to heavy energy demands that led to an increase in the consumption of fossil fuel and the elevation of pollution levels. However, many demands for exploration of new material with high-performance capability are in progress. Perovskites solar cells have been extensively investigated by researchers [1]. They have been considered later a better replacement for Si solar cells with a high chance for commercialization. Solar cell technology can be divided into two principal groups, crystalline cells and thin films. In the formers, the molecules are organized into crystalline grids, and can be divided into monocrystalline cells having a single-crystal structure and polycrystalline cells consisting of grids with different orientations [2]. The conduction mechanisms in these devices depend on various conditions such as surface preparation, interfacial layer, doping density and some electrical parameters like barrier height (B*o*), ideality factor (n), series resistance (R_s) and shunt resistance (R_{sh}), temperature, applied bias voltage and illumination intensity [3-7]. Grain boundaries in layered solar cells might also lead to both advantageous and disadvantageous effects. Several reports linked improved photovoltaic performance with the increase in grain size, however other reports revealed conflicting origins for this improvement [8-10]. Radiation has the ability to modify the characteristics of materials when irradiated using gamma rays and neutrons as non-ionizing radiation. Electronic features of a Schottky diode are also affected by many factors like temperature [11], humidity [12,13], and radiation [14]. When gamma radiation passes through a semiconductor device, different effects including defects such as vacancies, defect clusters, dislocation loops near the surface and variation of band gap width take place [15]. Many works have been reported for the effect of O_2, air and H_2 plasma on the PV efficiency [16-18]. The authors unveiled that H_2 plasma passivation of shallow and deep impurities in crystalline Si has led to intense interest in this area. Hydrogen plasma treatment is also found to improve the performance of polycrystalline and amorphous silicon cells and leads to the improvement of the Si-SiO_2 interface [18]. In this work, we systematically studied the impact of grain boundaries on the performance of the devices. So, two types of Si solar cells (monocrystalline and polycrystalline) were examined. The effect of grain boundaries on the PV characteristics was achieved experimentally through the calculation of B*o*, n, R*s* and R*sh*. Measurement of the I-V characteristics and

*Corresponding author E-mail: Kamilia_sedeek@azhar.edu.eg

determination of V*oc*, I*sc* and efficiency under different conditions were done also. The effect of gamma rays on cell parameters of both monocrystalline and polycrystalline Si cells was followed using a ^{60}Co gamma cell [2000 Ci] as a gamma-ray source. Also, the DPF was used to generate an ion beam with a kinetic energy ranging from 400 to 500 keV and a lifetime of about 200 ns. The DPF effect was followed on both cell types. An additional goal of this work is to improve the efficiency of the cells under study. So, a thin layer of ZnO (ZnO/Si) and SrTiO3 ($SrTiFeO_3$/Si) has been deposited into the front of the Si PV cell as an attempt to move the solar array towards absorbing longer solar irradiance for maximum power output.

2 Materials and experimental techniques:

2.1 Solar cell texture:

For the present work eight monocrystalline Si (JS158M5) solar cells and eight polycrystalline Si (LWP5BB-157) solar cells, each having dimensions 50*50 mm² were collected. These cells were fabricated by LIGHTWAY ENERGY TECHNOLOGY CO., LIMITED. For the monocrystalline cell, the product features are: Thickness (Si)= 190 ± 30 µm. Front: anisotropically texturized surface and dark silicon nitride (SiN) anti-reflection coatings, 0.7mm silver busbars. Back: local aluminum back surface-field, 1.8mm (silver / aluminum) discontinues soldering pads. The polycrystalline cell has a thickness of 200 ±20 µm. Front side: 0.7mm wide bus bars, silicon nitride anti-reflection coating and back side with 1.7mm wide bus bars, silicon nitride coating. Silicon nitride has been shown to provide very low surface recombination velocities on p-type and n-type wafers [19]. The second advantage is the antireflective properties of the nitride layer which reduce considerably the light reflection. Low resistance, not expensive and compatible Al ohmic contacts were welded on the wafer rear and front by rapid thermal annealing.

2. 2 Experimental Techniques:

For the solar cell characterization, the I-V data were experimentally collected to determine the parameters that characterize the cell. The I-V measurements were performed using a KEW 1011 digital multimeters at dark while the PV parameters measurements were carried out under direct sunlight illumination. The light intensity was measured by a digital meter model UT383S. To study the effect of gamma radiation on the cell efficiency, monocrystalline and polycrystalline cells were exposed each to two different doses. The selected cells were irradiated using a ^{60}Co Indian irradiator cell. A ^{60}Co gamma cell [2000 Ci] was used as the gamma-ray source at room temperature. The dose rate equaled 2.56 Gy/s, and the maximum total dose was 10 kGy. The I-V of irradiated cells was recorded immediately within 4h after removal from the radiation field. To follow the effect of atmospheric gases on the solar cell efficiency, the DPF was used to generate an ion beam with a kinetic energy ranging from 400 to 500 keV and a lifetime of about 200 ns. The DPF device is a type of plasma accelerator that produces nanosecond pulses. The cell was placed in the plasma chamber with nitrogen gas pressure of 2 mbar at 6 cm from the plasma focus (ion beam source). The number of shots was 10 and the charging voltage was 12 kV. In order to improve the Si solar cell efficiency, thin films of ZnO and SrTiO3 were deposited each as a front layer on the top of the anti-reflection coating (SiN) of the monocrystalline and polycrystalline cells. Film deposition was carried out using electron gun - LEYBOLDHERAEUS coating unit model COMBITRON CM30 at a pressure of $5x10^{-3}$ Pa and a rate of 1.5-2.5 nm/s. The deposited thickness was approximately 150 nm. A SEM model ZEISS EVO 15 was employed to collect the surface images and a spectrophotometer model Cary5000 double-beam spectrophotometer was used to measure the transmittance.

3 Result and discussion:

3. 1 Calculation of electrical and PV parameters:

The electrical behavior of a solar cell is represented by the practical equivalent circuit given in Fig. 1.

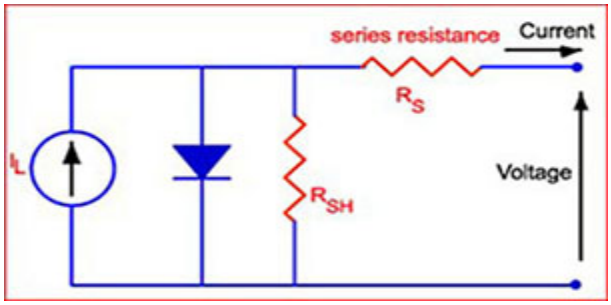

Fig. 1: I-V diode circuit presentation of a PV cell model

A set of both mono and polycrystalline Si solar cells were characterized at room temperature. The forward and reverse bias current-voltage (I-V) characteristics were carried out at dark. Fig.2-a, b displays the I-V curves chosen as representative of the general electrical trend of the contact. As can be seen, the cells show good rectifying behavior. The current shows weak voltage dependence in the reverse bias especially for the monocrystalline cell and an exponential increase in the forward bias which is the characteristic properties of good rectifying contacts [20].

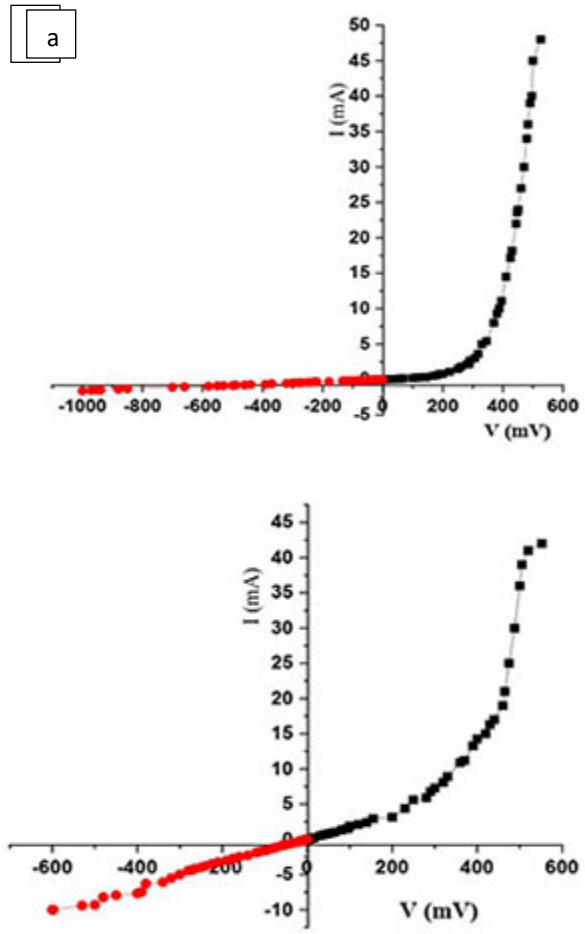

Fig. 2: I-V curves for forward and reverse bias measured at dark for a) monocrystalline and b) polycrystalline solar cells

The I-V characterization of the Si photovoltaic cells under forward bias was performed in order to determine the parameters that regulate the flow of current across the junction - contact, namely: *n, Bo , Rsh and Rs.* The presence of the series resistance causes the ideality factor (n) of a diode to take a value greater than unity. In this case, the relation between current and applied voltage can be expressed by the modified thermionic emission theory as [21-23]:

$$I = I_o \exp [\, q\,(V - IRs) / n\,kT\,] \; [\; 1 - \exp - q\,(V - IRs)\,/kT\,] \quad (1)$$

Where V is the applied bias voltage, T is the temperature in K, k is the Boltzmann constant, and I_o is the reverse bias saturation current.

The value of Io can be extracted from the straight-line intercept of ln(I)-V plot at zero-bias and is given by:

$$I_o = AA^*T^2 \exp (-q\,B_o / kT) \quad (2)$$

Where A is the effective diode area, A^* is the Richardson constant [24] and B_o is the zero-bias apparent barrier height.

Once Io is determined B_o can be calculated by rewriting Eq. (2) as:

$$B_o = (kT/q) \ln [AA^*T^2 / I_o\,] \quad (3)$$

In order to calculate the deviation of the experimental I-V data from the ideal thermionic theory, the value of n was determined by calculating the slope of the linear portion of the forward bias region in the ln I versus V plot and this can be expressed as: [21, 22]

$$n = q/\,kT\,[\mathrm{d}\,(V - IRs)\,/\,\mathrm{d}\,(\ln I\,)\,] \quad (4)$$

Fig. 3-a, b depicts the semi-logarithmic plot of the forward and reverse bias I-V curves measured for mono and polycrystalline cells. As can be seen, each forward bias semi-logarithmic I-V plot consists of a wide linear range in the intermediate bias region (0.1 - 0.5 V). However, in the reverse bias, the current increases slowly then tend to saturate for both monocrystalline and polycrystalline cells. The experimental values of Bo and n are respectively 0.61 eV, 0.62 eV and, 2.75, 3.55 for mono and polycrystalline cells (table 1). Similar, high values of n have been also reported [25]. The deviation of the ideality of the solar cell and the high value of n can be attributed to the generation-recombination current within the space charge region and to the presence of interface states at metal/semiconductor interface [26-28], in addition to the image force lowering of the barrier height [29].

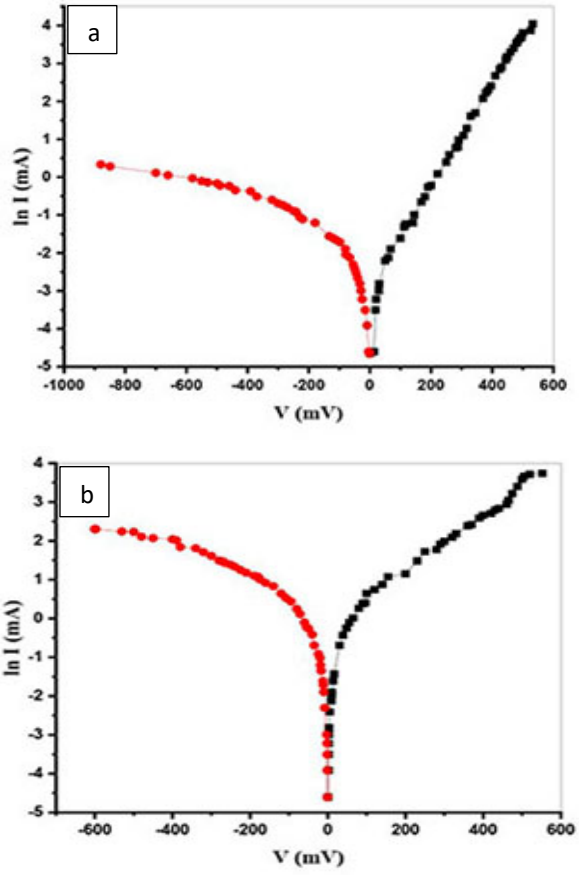

Fig. 3: Relation between (V) and Ln (I) for forward and reverse biased a) monocrystalline and b) polycrystalline

solar cells.

3. 2 Resistance measurement

Due to the high defect and impurity accumulated at the grain boundaries specially in polycrystalline PV cells, the photo-generated charge carriers will recombine strongly at the boundaries. The defects result in deep energy levels in the forbidden band gap and act as recombination centers in any semiconductor material and cause electrical losses. There are two types of resistance in the diode unit: the series resistance (resistance of hole and electron motion) and the parallel resistance or shunt resistance (recombination of holes and electrons). It is known that the shunt resistance is defined as the inverse slope of the I-V curve at the 0 V point. However, the light input must be constant for the calculation to be consistent with the theoretical model [30]. The practical method to determine (R*s*) and (R*sh*) is to plot the structure resistance (R*i*) versus applied bias voltage (V). R*i* is determined from the I–V characteristics by using Ohm's law *(* R*i* = dV/di). In this method, at sufficiently high forward bias voltage the structure resistance approaches to a constant value which is equal to the series resistance. Also, at sufficiently high reverse bias voltage, the structure resistance reaches a constant value equal to structure shunt resistance [31]. Fig.4-a, b illustrates the plot of R*i* versus V for both mono and polycrystalline solar cells under study. The calculated values of R*s* and R_{sh} are 11 ohm and 678 ohm, and 12 ohm and 74 ohms respectively for monocrystalline and polycrystalline cells as given in table 1. In general, the small value of *Rs* and the high value of R_{sh} are a mirror of PV cell goodness.

Table 1: values of n, B_o, R*s*, and R*sh* for monocrystalline and polycrystalline Si PV cells under study.

Type	n	B*o* (eV)	R*s* (ohm)	R_{sh} (ohm)
Monocrystalline	2.75	0.61	11	678
Polycrystalline	3.55	0.62	12	74

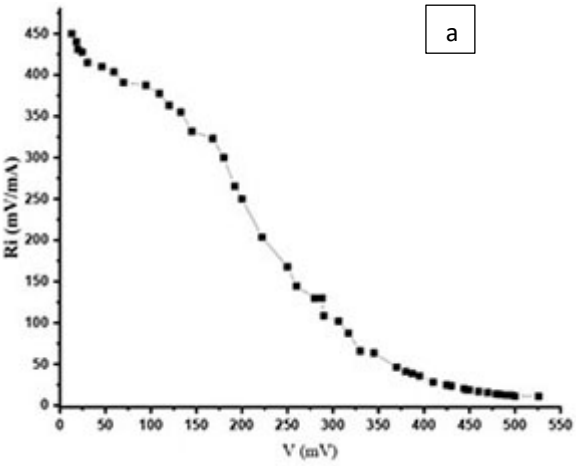

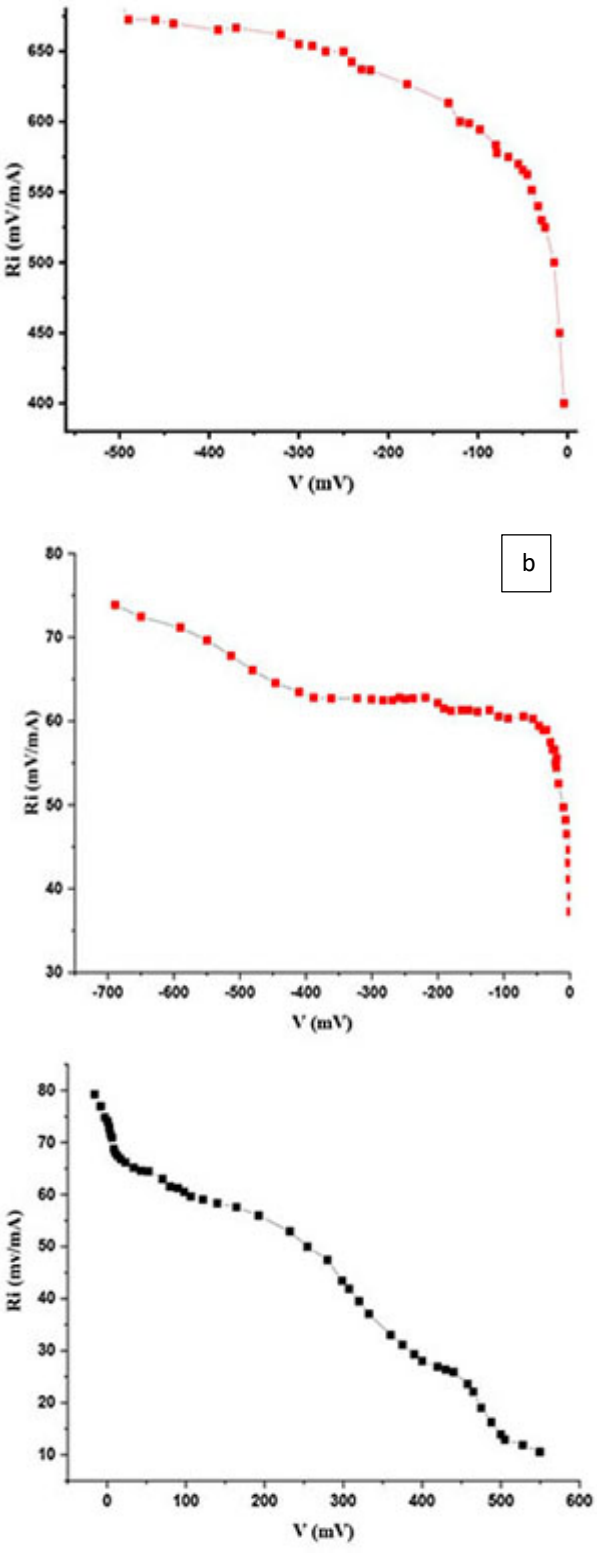

Fig. 4: Plot of the variation of the resistance Ri versus the applied voltage V for a) monocrystalline and b) polycrystalline solar cells.

- Solar cell efficiency calculation

For a given solar spectrum, the efficiency depends on: the

semiconductor material, device structure, ambient conditions, high radiation damage and sun spectrum. Efficiency alone is not enough; the cost of the cell and the lifetime are also important.

To calculate the efficiency of a solar cell the following formula can be used [32]:

$$\eta = Pm / Pin \quad (5)$$

$$Pm = Vmp * Imp$$

$$\eta = [\ Voc * Isc * FF\ ] / Pin \quad (6)$$

Where *Pin* is the input power (the lux intensity in W/m^2).

The *FF* factor is a graphical representation of the "squareness" of the solar cell characteristic and is expressed by:

$$FF = (Imp * Vmp) / (Isc * Vsc) \quad (7)$$

Tables 2-5 give the calculated values**.**

3. 3 Effect of gamma rays

According to Lambert-Beer law, a collimated mono-energetic gamma ray beam attenuates in matter according to [33]:

$$| = |_o\ e^{-\mu t} \quad (8)$$

Where $|_0$ is the gamma ray initial intensity, | is its intensity following attenuation through a sample of thickness *t* (cm), and μ (cm^{-1}) is the material linear attenuation coefficient. The effect of gamma ray absorption has been revealed through the I-V measurements. Fig.5-a,b illustrates the photovoltaic I-V curves for a mono and a polycrystalline Si solar cell before and after exposure to two different doses.

Radiation has the ability to modify the characteristics of materials when irradiated using gamma rays and neutrons.

As shown in table2, gamma irradiation at 1kGy results in an increase of *Voc and Isc* which in turn results in an improvement of the maximum power and the efficiency for both types of cells. However, this improvement is more pronounced for the mono cell, η is nearly increased by more than 40% upon exposure to 1kGy dose. On the other hand, exposure to 10kGy has lower effect; even both cells become crispy after irradiation. As reported, electronic features of a Schottky diode described as its barrier height, ideality factor and series resistance parameters are affected by gamma rays [34-36]. Actually, different effects including defects such as vacancies, defect clusters, dislocation loops near the surface and variation of band gaps width take place [37].

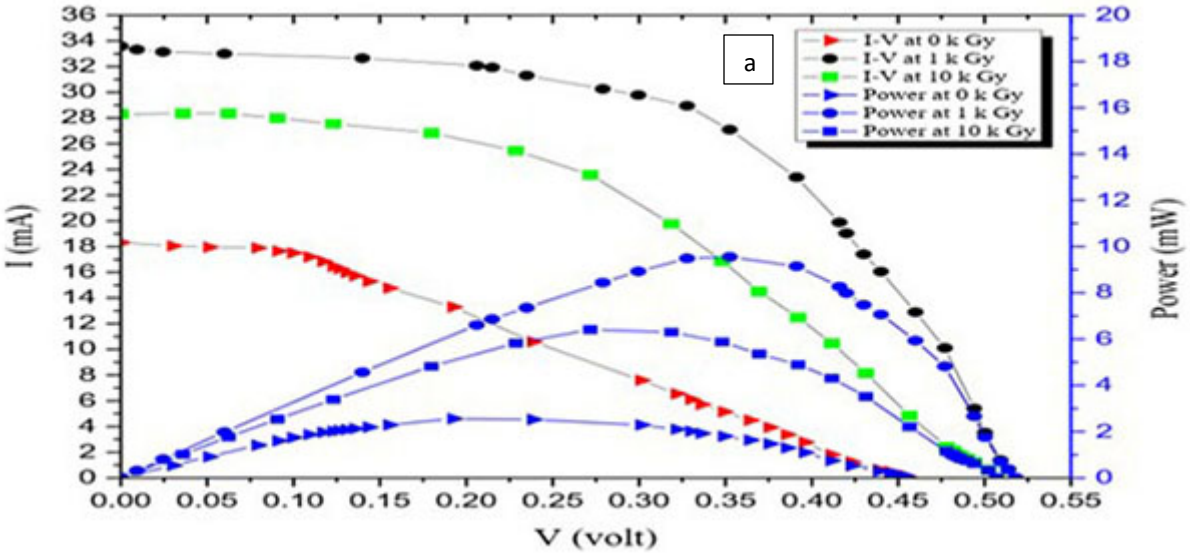

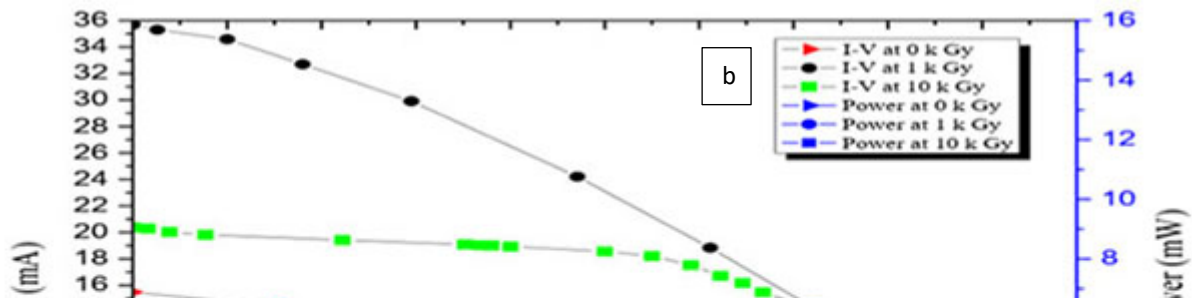

hing Cor.

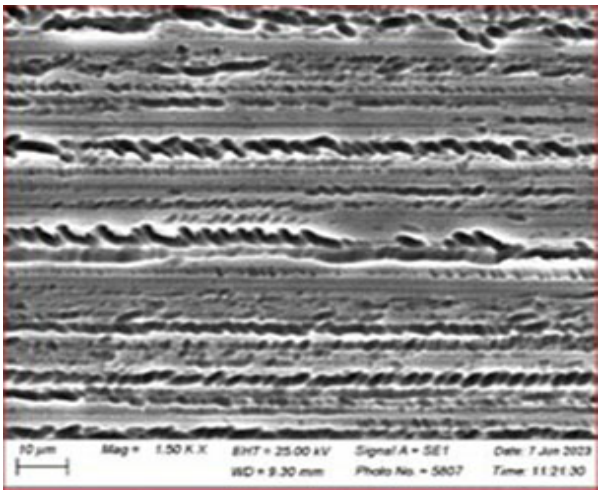

Fig. 6: SEM for polycrystalline Si solar cell a) before and b) after DPF.

Table 2: V_{oc}, I_{sc} and efficiency for monocrystalline and polycrystalline solar cells before and after different doses of radiation.

Cell	V_{OC} (mV)	I_{SC} (mA)	η%	FF%
Mono. at 0 Gy	459	18.3	16.7	50
Mono. at 1k Gy	518	33.6	24.0	59
Mono. at 10k Gy	507	28.4	22.1	52
Poly. at 0 Gy	463	15.5	14.9	48
Poly. at 1k Gy	500	35.7	19.8	51
Poly. at 10k Gy	478	20.4	18.0	50

3. 4 Effect of plasma exposure

The effect of plasma exposure on the texture and the surface morphology of the cells have been followed using the SEM. Fig. 6-a,b gives, as an example, the SEM image for the polycrystalline Si solar cell before and after exposure. As shown, the surface image of the unexposed polycrystalline Si cell does not show any landmarks. Exposure to plasma seems however to create some sort of surface texture with the formation of aligned grains.

To investigate the effect of plasma on the solar cell efficiency, measurements of the I-V curves have been carried out before and after plasma exposure. Fig.7-a, b shows the I-V plots while table 3 gives the calculated photovoltaic parameters for mono and polycrystalline Si cells before and after plasma exposure. It is clear that exposing the cell surface to plasma does not cause any damage but, in the contrary, it improves its efficiency by 16.5 % and 22 % respectively for monocrystalline and polycrystalline cells. Hydrogen is able to migrate in c-Si and to bond to both shallow and deep level impurities, passivating their electrical activity [38]. The effect of Hydrogen on polycrystalline or damaged Si was reported [39]. The authors predicted that hydrogen plasma treatment leads to an improvement in the performance of solar cells with grain boundaries and inter-grain defects that become electrically inactive. Seager et al. [40] concluded that the improvement results from removal of the inter-grain trapping states, while Ammor et. al. [41] declared that the interfacial recombination velocity at grain boundaries decreases causing the effective diffusion length to increase after hydrogenation.

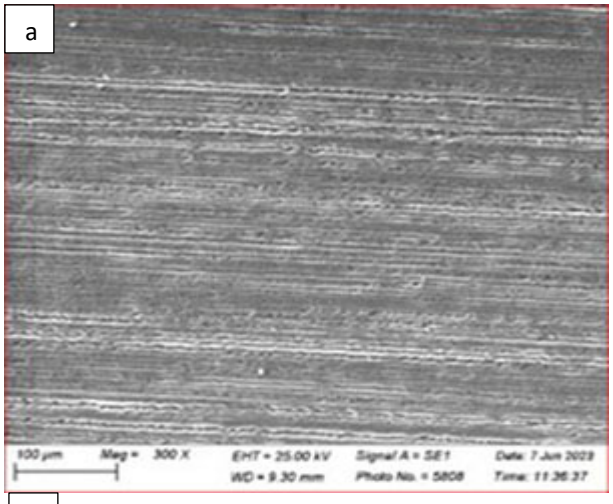

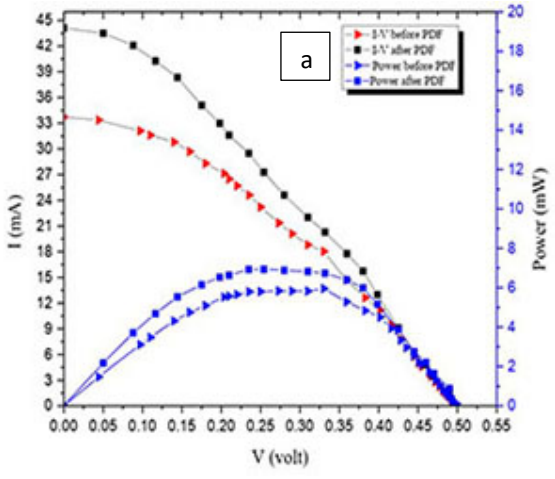

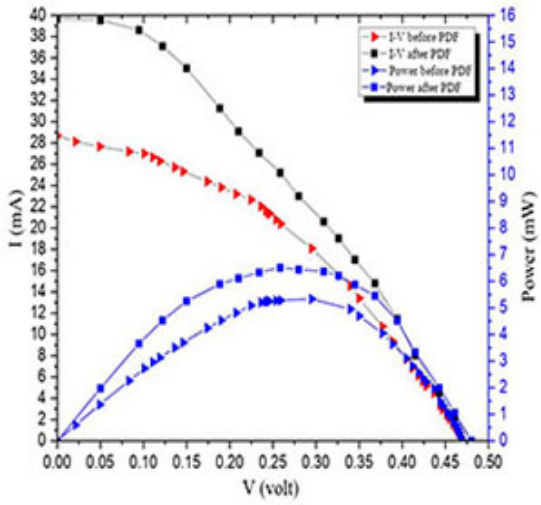

Fig. 7: I-V plot for a) monocrystalline and b) polycrystalline Si solar cell before and after DPF.

Table 3: $V_{oc,}$ $I_{sc\ and}$ efficiency for monocrystalline and polycrystalline solar cells before and after DPF exposure.

Cell	V_{OC} (mV)	I_{SC} (mA)	η%	FF%
Mono. before	497	33.7	20.6	55
Mono. after	500	44.1	4.0 24.0	28. 62
Poly. before	470	28.7	18.2	50
Poly. after	480	39.7	22.3	54

3. 5 Effect of thin film deposition

The photovoltaic performance of a Si solar cell can be improved by depositing a surface layer at the top of the cell. In such a case, this layer can be used as an absorber and a carrier transporter simultaneously. Materials with wide optical band gaps are usually chosen. This improves both the light absorption and the charge transport while considerably diminishes charge carrier recombination at the cell surface. Zinc oxide as one of the groups II–VI binary semiconductors characterized by wide and direct bandgap, high electron mobility and thermal stability has been used in different photo-electronic applications [42, 43]. ZnO is more selected for energy applications as it is environmentally friendly and cost-effective. It is used as the active layer in p-n or n-n hetero-junction and also as antireflection coating in hetero-junction solar cells [44,45]. It can also be coupled with smaller energy gap semiconductors such as Si and GaAs to extend their light absorption to the visible region. On the other hand, recent research focused also on the development of perovskite solar cells as their efficiency has significantly jumped from 3.8% to 20.7% in less than ten years [46]. Perovskite is a class of compounds with the general formula ABX_3, where A and B are cations with different sizes, and X is an anion. $SrTiO_3$ is an n-type semiconductor with cubic perovskite structure [47, 48]. They are metal oxides with peculiar charge ordering that leads to their multifunctional and diversified applications such as in solar cells [49]. So, ZnO and $SrTiO_3$ have been chosen through the present work as an active layer for Si based solar cell.

To measure the optical band gap width of the deposited ZnO and $SrTiO_3$ layers, a glass substrate was placed near the Si cell inside the electron beam gun unit during each run. Fig.8-a presents the optical transmittance spectra of ZnO and $SrTiO_3$ thin films measured at room temperature. Clearly, ZnO is more transparent. The optical band gap (Eg) of the films deposited on glass was calculated using the formula [50]:

$$\alpha h\upsilon = B\,(h\text{-}Eg)^m \qquad (9)$$

where B^{-1} is the edge width parameter related to the degree of randomness of the network, α is the absorption coefficient and m determines the nature of the transition. m = 1/2 or 2 for allowed direct or allowed indirect transitions respectively. It is well known that ZnO has an allowed direct band gap, so m = 1/2 has been manipulated for band gap calculation. The plot of $(\alpha h\upsilon)^2$ versus $h\upsilon$ is given in Fig. 8-b. The optical band gap width is determined by extrapolating the linear portion of the curve to the x axis at $\alpha h\upsilon = 0$. The determined values of Eg are respectively 3.03eV and 3.52 eV for ZnO and $SrTiO_3$. Such values qualify these films to act as a window for collecting more solar radiation. Other workers published similar values of Eg [51,52].

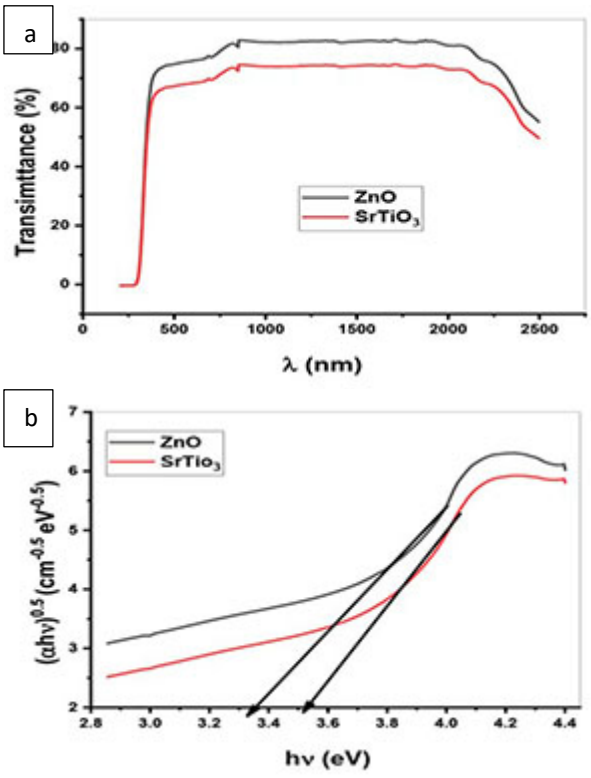

Fig 8: (a) The transmittance spectra of the deposited ZnO and $SrTiO_3$ thin films; (b) The optical band gap (Eg) of the deposited ZnO and $SrTiO_3$ thin layers.

3.5.1 I-V characteristic for ZnO/Si solar cell:

To image the surface morphology changes after ZnO

deposition, the SEM was employed. As mentioned above, the image of the uncovered polycrystalline Si cell does not have any definite landmarks (Fig. 9-a) while the image of the uncovered monocrystalline surface appears smoother (Fig.10-a) without indication of grains.

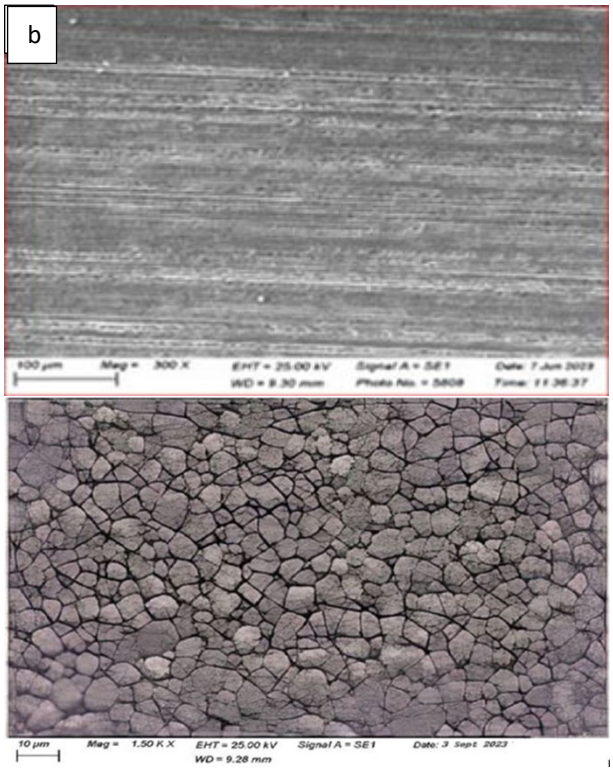

Fig 9: SEM of polycrystalline solar cell a) before and b) after ZnO deposition

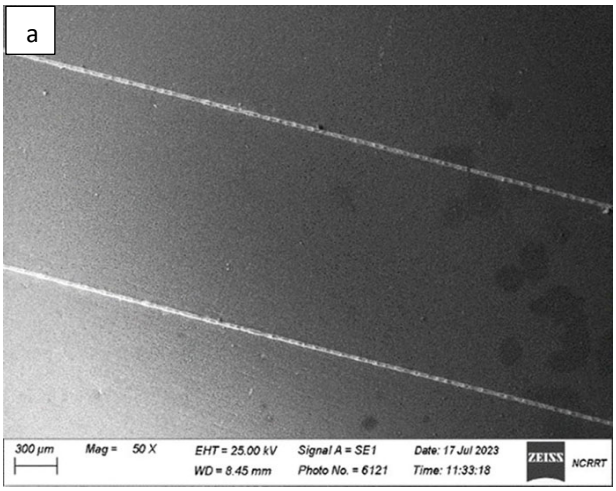

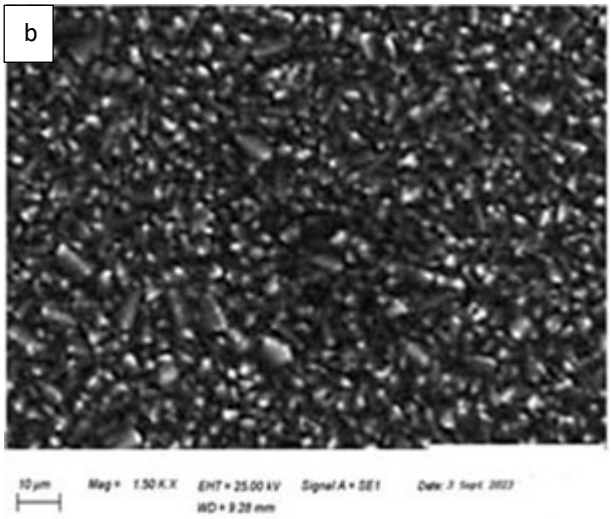

Fig. 10: SEM of monocrystalline solar cell a) before and b)) after ZnO deposition

The deposited layer of ZnO at the front surface of the two types of cells has been imaged. The SEM of ZnO/poly-Si shows dense distribution of semi-spherical grains as shown in Fig.9-b while that of ZnO/mono Si gives an image of dense distribution of rod-like particles arranged in different orientations (Fig.10-b). The photovoltaic I-V curves measured for monocrystalline and polycrystalline ZnO/Si in comparison with Si solar cells are displayed in Fig. 11 and 12, while table 4 gives the calculated parameters. It is clear that for both types a great increase in the efficiency takes place especially for the ZnO/mono-Si solar cell where an increase by about 50% occurred**.**

Following the work of OJO and Dharmadasa [53], a schematic representation of the graded bandgap structure of the multilayer monocrystalline Si solar cell under study is drawn and illustrated in Fig. 13. ZnO as an n-type intrinsic semiconductor (Eg ≈ 3.03 eV), apart from being a window and absorber front layer it acts as a hole back diffusion barrier (hbdb) layer [53-57]. It minimizes the recombination of photo-generated holes, push them back to the Al back contact. SiN as a second layer (Eg ≈ 2.73 eV) is reported as a good charge storage material that improve the performance of multi-crystalline solar cells (19). Improving the photovoltaic performance of the Si solar cell is therefore expected by ZnO deposition. The moderate increase in the efficiency of the ZnO /Poly-Si (14.5%) can be attributed to the fact that polycrystalline structure is characterized by grain boundaries, so electrons suffer many trapping/detrapping actions while traversing the junction [58,59]. This slows down the electron transfer, so lower improvement takes place for polycrystalline cells as shown in table 4.

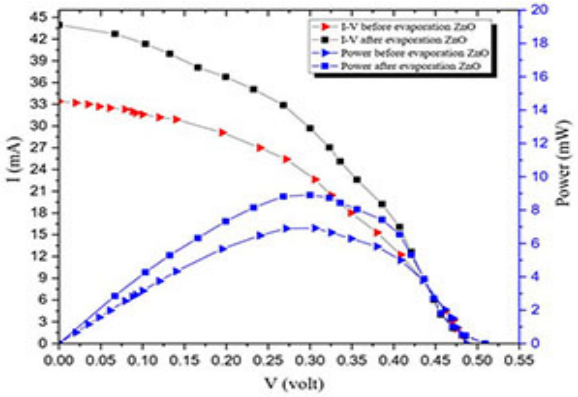

Fig. 11: Plot of I-V for monocrystalline solar cell before and after ZnO deposition

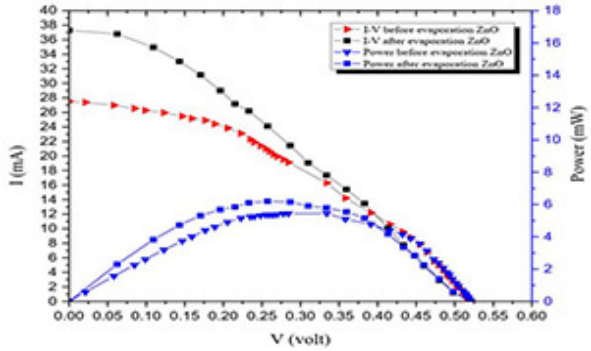

Fig. 12: Plot of I-V for polycrystalline solar cell before and after ZnO deposition

Table 4: V_{oc}, I_{sc} and efficiency for monocrystalline and polycrystalline solar cells before and after evaporation of ZnO.

Cell	V_{OC} (mV)	I_{SC} (mA)	η%	FF%
Mono.before	487	33.4	20.0	60
Mono.after	509	44.0	24.6	68
Poly.before	521	27.5	18.6	51
Poly. after	520	37.3	21.3	56

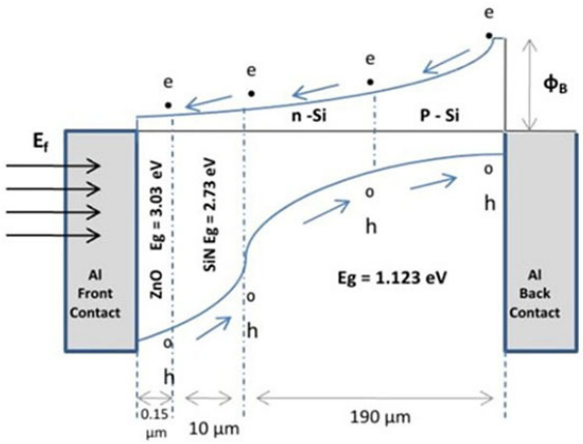

Fig. 13: A schematic representation of the graded band gap

diagram of the multilayer monocrystalline Si solar cell under study.

3.5.2 I-V characteristic for SrTiO3/Si solar cell

The texture and the morphology of the $SrTiO_3$/Si surface have been imaged by SEM. The image reveals a regular distribution of pyramid-shaped perovskite particles covering the surface of the $SrTiO_3$ /mono-Si. On the other hand, the $SrTiO_3$/poly-Si shows coverage of perovskite layer consisting of non-uniform distribution of nano-rods interspersed with pores as displayed in Fig. 14-a, b and 15-a, b.The I-V curves for monocrystalline and polycrystalline solar cells before and after evaporation of $SrTiO_3$ are shown in Fig.16 and 17. As shown in table 5, the efficiency increases respectively by 24 % and 26 % for monocrystalline and polycrystalline $SrTiO_3$/Si cells. SrTiO3 is a metal oxide with peculiar charge ordering that leads to its use as a preferred material for manufacturing solar cells [60].

It exhibits a ferroelectric nature which is responsible for a suitable behavior at the above band gap voltage. This PV effect appears at the ferroelectric domain boundaries by the separation of charges to generate a photocurrent [61].

Furthermore, the presence of perovskite as a passivation front layer is reported to improve the photovoltaic behavior of the solar cell by preventing the surface recombination of minority carriers (holes), due to the creation of positive electric field at the perovskite/silicon interface [62].

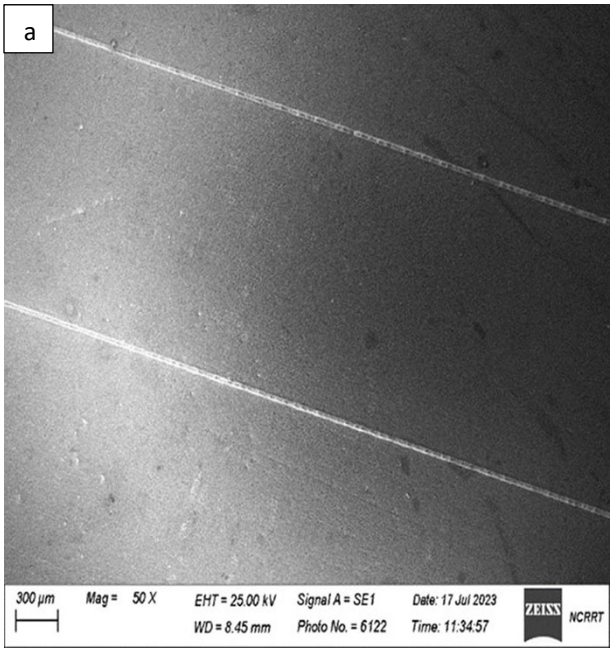

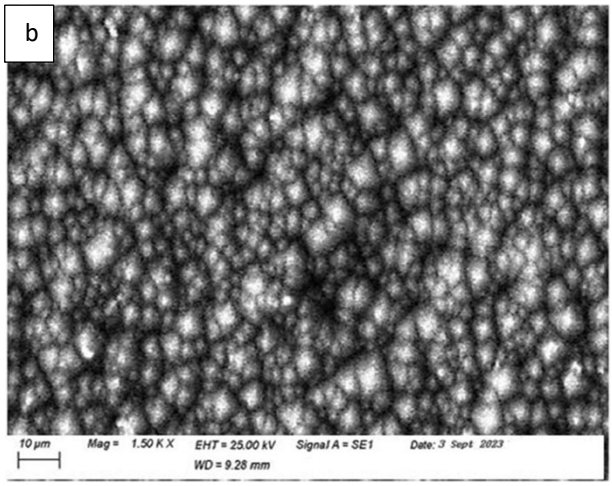

Fig. 14: SEM of monorystalline solar cell a) before and b) after SrTiO3 deposition

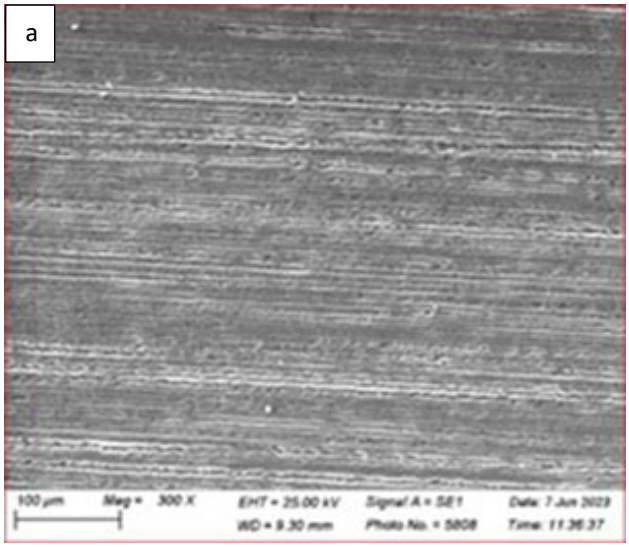

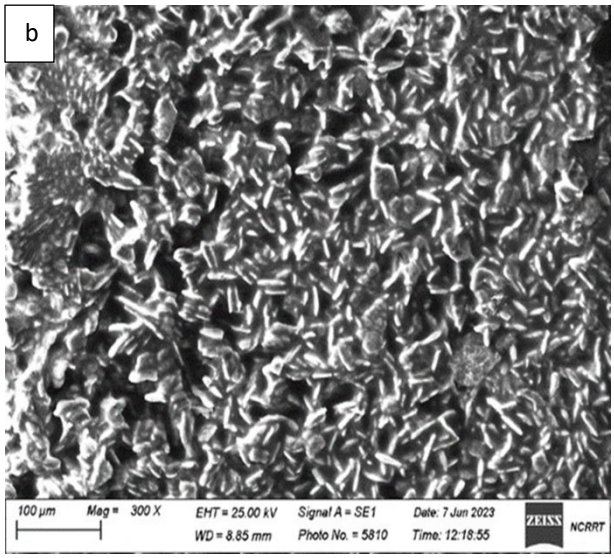

Fig. 15: SEM of polycrystalline solar cell a) before and b) after $SrTiO_3$ deposition

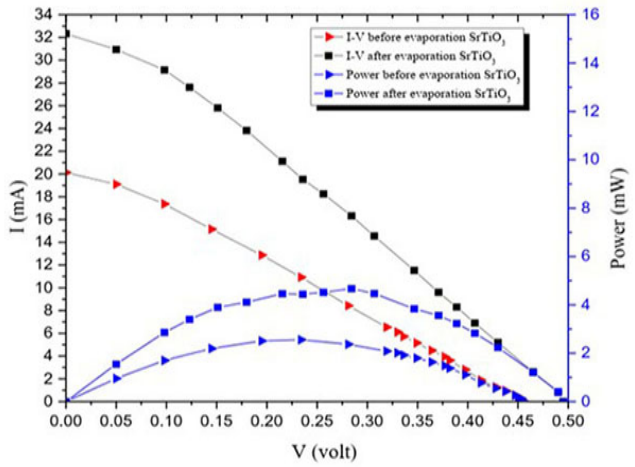

Fig. 16: I-V plot of monocrystalline solar cell before and after $SrTiO_3$ deposition

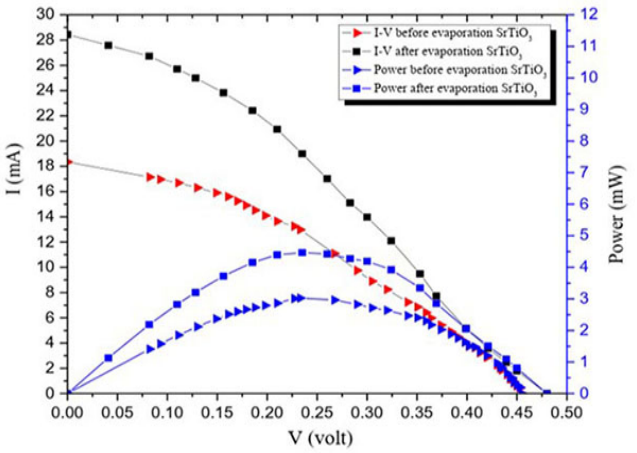

Fig. 17: I-V plot of polycrystalline solar cell before and after $SrTiO_3$ deposition

Table 5: V_{oc}, $I_{sc.\ and}$ efficiency for monocrystalline and polycrystalline solar cells before and after evaporation of $SrTiO_3$

Cell	V_{OC} (mV)	I_{SC} (mA)	η%	FF%
Mono.before	456	20.1	16.4	52
Mono. after	495	32.2	20.4	58
Poly. before	455	18.3	15.3	50
Poly. after	480	28.5	19.5	54

Conclusion:

This work aimed to study the effect of surrounding atmosphere namely gamma rays and H2 plasma on the efficiency of solar cells. Improvement of the device performance has been also followed by depositing a ZnO or $SrTiO_3$ layer at the cell front surface. So, some commercial monocrystalline and polycrystalline Si solar cells were collected. The work started by measuring the current–voltage (I-V) characteristic. The results were analyzed

using the conventional thermionic emission theory to estimate the barrier height, ideality factor, series and shunt resistances. An increase of the efficiency for both cell types was detected using two different doses (1kGy and 10 kGy) of gamma rays. To follow the impact of atmospheric gases (H2) on the solar cell efficiency, the dense plasma focus was used. The SEM was employed to image the cell surface before and after front layer deposition. A pyramid-like texture of the SrTiO3/mono-Si and a rod-like texture of the ZnO/mono-Si surfaces were formed. For both cells, an efficiency improvement resulted. it was found that the formation of the hierarchical texture of SrTiO3/mono-Si and the rod-like texture of ZnO/mono-Si surfaces improve the photoelectric response as they act as electron carrier materials that extract and transfer image-generating electrons.

Statements and Declarations

Compliance with Ethical Standards

Funding: The authors declare that no funds, grants, or other support were received during the preparation of this manuscript.

Competing interests: The authors have no relevant financial or non-financial interests to disclose.

Research Data Policy and Data Availability

The authors declare that the data supporting the findings of this study are available within the paper.

Author Contributions

All authors contributed to the study conception and design. K. Sedeek and H.A. Saudi wrote the main manuscript text, revised the experimental and calculated data. Gh. A. Al-zaidi, and M. S. Shalaby carried out the experimental part and calculations, Ibrahim A. Nassar revised the whole text.

References

[1] Krishnan U., Kaur M., Kumar M., Kumara A., “Factors affecting the stability of perovskite solar cells: a comprehensive review,” J. Photon. Energy 9(2), 2019, 021001.

[2] Kobougias I., Tatakis E., and Prousalidis J., PV Systems Installed in Marine Vessels: Technologies and Specifications. Advances in Power Electronics, 2013.

[3] Sze S. M, Physics of Semiconductor Devices, 2 ed., Willey & Sons, New York, 1981.

[4] Rhoderick E. H., Williams R. H., Metal Semiconductor Contacts, 2 ed., Clarendon, Oxford, 1988.

[5] Arslan E., Altındal S., Özçelik S., Özbay E., Tunneling current via dislocations in Schottky diodes on AlInN/AlN/GaN heterostructures Semiconductor Science Technology, 24, 2009, 075003.

[6] Demirezen S., Altındal S., Possible current-transport mechanisms in the (Ni/Au)/Al0.22Ga0.78N/AlN/GaN Schottky barrier diodes at the wide temperature range, Current Applied Physics, 10, 2010, 1188.

[7] Tunç T., Altindal Ş., Dökme I., Uslu H., “The anomalous peak in the forward bias C-V plot and temperature dependent of interface states and series resistance of Au/PVA (Ni,Zn-doped)/n-Si (111) structures, "Journal of Electronic Materials, 40 , 2011, 157.

[8] Qingzhi A., Fabian P., David B., Changsoon C., Qing S., Andreas W., Sapir B., Nir T., and Yana V., Small grains as recombination hot spots in perovskite solar cells, Matter. 4, 2021, 1683.

[9] Jariwala S., Sun H., Adhyaksa G.W., Lof A., Muscarella L.A., Ehrler B., Garnett E.C., and Ginger D.S. Local crystal misorientation influences non-radiative recombination in halide perovskites, 2019, 3048.

[10] Olyaeefar B., Ahmadi-Kandjani S., and Asgari A. , Classical modelling of grain size and boundary effects in polycrystalline perovskite solar cells. Sol. Energy Mater. Sol. Cells 180, 2018, 76.

[11] Aydoğan ÖG Ş. , Türüt A. Fabrication an electrical properties of Al /aniline green/n-Si/Au Substructure, Materials Science in Semiconductor Processing, 11(2), 2008, 53.

[12] Jo Y-S, Lee Y., Roh Y. Effects of humidity on the electrical conduction of lambda-DNA trapped on a Nano-gap Au electrode. Journal of the Korean Physical Society, 43(2), 2003, 909.

[13] Otsuka Y., Lee H-y, Gu J-h, Lee J-O, Yoo K-H, Tanaka H., et al. Influence of humidity on the Electrical Conductivity of synthesized DNA film on nanogap electrode. Japanese journal of applied physics, 41(2R), 2002, 891.

[14] Jayavel P., Kumar J., Santhakumar K., Magudapathy P., Nair K. Investigations on the effect of alpha particle irradiation-induced defects near Pd/n-GaAs interface. Vacuum, 57(1), 2000, 51.

[15] Gupta RK, Yakuphanoglu F. Photoconductive Schottky diode based on Al/p-Si/SnS2/Ag for optical Sensor applications. Solar Energy. 86(5), 2012, 1539.

[16] Chang K. J. and Chadi D.J.,Theory of the Atomic and Electronic Structure of DX Centers in GaAs and $Al_xGa_{1-x}As$ Alloys, Phys. Rev. Lett.61, 1988, 873.

[17] KassabovJ. J., Dimitrov D., and Grueva A., Acceptor states at the $SiSiO_2$ interface generated by UV and their effect on electron mobility, Solid State electronics Vol. 31, 1988.

[18] Schmalz K., Kirscht F. G., Klose H., Richter H. and Tittelbach-Hermrich K., DLTS study of deep level defects in Cz n-Si due to heat treatment at 600 to 900 °C Phys. Stat. Sol. (a), 100 (2),1987, 567.

[19] El amrania A., Menousa I., Mahiou L., Tadjineb R., Touatia A., Lefgouma A., Silicon nitride film for solar cells, Renewable Energy, 33, 2008, 2289.

[20] Janardhanam V., Kumar A. A., Reddy V. R.,S Reddy P. N., Study of current–voltage–temperature (I–V–T) and capacitance–voltage–temperature (C–V–T) characteristics of molybdenum Schottky contacts on n-InP (100), J. Alloys and Compounds, 485, 2009, 467.

[21] Uslua, A. Bengi , Etina S.S., Aydemir U., Altındal S., Aghaliyeva S.T., Özc S., Elika S., Temperature and voltage dependent current-transport mechanisms in GaAs/AlGaAs single-quantum-well, J. Alloys and Compounds, 507, 2010, 190.

[22] Lee C.C., Chen W.V., Park J., A new I–V model for light-emitting devices with a quantum well. Microelectronics Journal, 37, 2006, 1335.

[23] Chen C.H., Baier S.M., Arch D.K., Shur M.S., A new and simple model for GaAs heterojunction FET gate characteristics, Electron Devices 35, 1988, 570.

[24] Neil W.Ashcroft, David Mermin, Solid State Physics, New York: Standard recording College Publishing, 1976, 362

[25] Altındal S., Dökme I., Bülbül M.M., Yalc N., Serin T., The role of the interface insulator layer and interface states on the current-transport mechanism of Schottky diodes in wide temperature range Microelectronics, Eng. 83, 2006, 499.

[26] Cova P., Singh A.,Temperature dependence of I-V and C-V characteristics of Ni/n-CdF2 Schottky barrier type diodes Solid State Electron. 33, 1990, 11.

[27] Card H.C., Rhoderick E.H., Studies of tunnel MOS diodes I. Interface effects in silicon Schottky diodes, J. Phys. D. Appl. Phys. 4, 1971, 1589.

[28] Singh A., Reinhardt K.C., Anderson W.A., Temperature dependence of the electrical characteristics of Yb/p-InP tunnel metal-insulator-semiconductor junctions, J. Appl. Phys. 68, 1990, 3475.

[29] Divigalpitiya W.M.R, Temperature dependence of the photovoltaic characteristics of silicon MIS solar cells, Sol. Energy Mater. 4, 1989, 253

[30] Paul R. Thompson and Thomas C. Larason, METHOD OF MEASURING SHUNT RESISTANCE IN PHOTODIODES. Measurement Science Conference 2001, Anaheim, CA, January 2001,

[31] Çetinkaya H. Tecimer , H. Uslu S., Altındal, silicon nitride film for solar cells, Renewable Energy, 33, 2008.

[32] Sze S.M., Physics of Semiconductor Devices, third ed., John Wiley&Sons, New York, 2007.

[33] Kassab L.R.P., Issa S.A.M., Mattos G.R., AL Misned G., Bordon C.D.S., Tekin H.O., Gallium (III) oxide reinforced novel heavy metal oxide (HMO) glasses: A focusing study on synthesis, optical and gamma-ray shielding properties, Ceram. Int. 48, 2022, 14261.

[34] Jo Y-S, Lee Y., Roh Y. Effects of humidity on the electrical conduction of lambda-DNA trapped on a Nano-gap Au electrode. Journal of the Korean Physical Society. 43(2), 2003, 909.

[35] Otsuka Y., Lee H-y, Gu J-h, Lee J-O, Yoo K-H, Tanaka H., et al. Influence of humidity on the Electrical Conductivity of synthesized DNA film on nanogap electrode, Japanese Journal of Applied Physics. 41(2R), 2002, 891.

[36] Jayavel P., Kumar J., Santhakumar K., Magudapathy P., Nair K. Investigations on the effect of alpha particle irradiation-induced defects near Pd/n-GaAs interface, Vacuum. 57(1), 2000, 51.

[37] Gupta RK, Yakuphanoglu F. Photoconductive Schottky diode based on Al/p-Si/SnS2/Ag for optical Sensor applications. Solar Energy, 86(5), 2012, 1539.

[38] Hao Qu, Gao Zhao, Yumeng Wang, Lijuan Liang, Long Zhang, Wenya Liu, Chunmei Zhang, Chen NiuI, Yi Fang, Jiushan Cheng and Dongdong Wang, Plasma-Exposure-Induced Mobility Enhancement of LiTFSI-Doped Spiro-OMeTAD Hole Transport Layer in Perovskite Solar Cells and Its Impact on Device Performance‹, Materials , 12(19) , 2019, 3142.

[39] Seager C.H., and Ginley D.S., Studies of the hydrogen passivation of silicon grain boundaries, J. Appl. Phys. 52(2), 1981, 1050.

[40] Seager C.H., Ginley D.S. and Zook J.D., Improvement of polycrystalline silicon solar cells with grain-boundary hydrogenation techniques, Appl. Phys. Lett. 36(10), 1980, 831.

[41] Ammor L. and Marionuzzi S., Influence of hydrogen implantation on properties of n+p polycrystalline silicon solar cells, Solid State Electronics, vo1.29, 1986, 1.

[42] Khan Z.R., Khan M.S., Zulfequar M., and Khan M.S., “Optical and structural properties of Zno thin films fabricated by sol-gel method,” Mater. Sci. Appl. 2, 2011, 340.

[43] Saito M.and Fujihara S., “Large photocurrenr generation in dye-sensitized Zno solar cells,” Energ.

Environ. Sci. 1, 2008, 280.

[44] Hussain B., Ebong A. and Ferguson I., "Zinc oxide as an active n-layer and antireflection coating for silicon based solar cell," Sol. Energ. Mat. Sol. Cells 139, 2015, 95.

[45] Caglar O., Carrot P., Losio P.A., Sinicco I., Nanocrystalline zinc oxide for surface morphology control in thin film silicon solar cell, 144, 2016, 55.

[46] Designing V.V. , Ravikumar C.R., Anil Kumar M.R., Suresh Ghotekar, Naveen Kumar A., Jahagirdar A.A., H.C. Ananda Murthy H.C., Structure, morphology and electrochemical properties of SrTiO3 perovskite: Photocatalytic and supercapacitor applications, Environmental Chemistry and Ecotoxicology 3, 2021, 241.

[47] Osman B.A., Abdolkader T.M., Ahmed I.S., A Review of Perovskite Solar Cells,International Journal of Materials Technology and Innovation Volume 1, Issue 2 , 2021, 48.

[48] Sedeek K., Said S.A., Hantour H., Makram N., and Amer T.Z., "Innovative synthesis and properties of Fe doped nanocrystalline strontium zirconate for the development of visible light driven photocatalyst," Results Phys., vol. 12, 2018, 1038.

[49] Bera A., Wu K., Shaikh A., Alarousu E., Mohammed O.F., Wu T., Perovskite oxide $SrTiO_3$ as an efficient Electron transporter for hybrid Perovskite solar cells, J. Phys. Chem. C, 118, 2014, 28494.

[50] Pankove J.I., Optical Processes in Semiconductors, I Dover, I New York, 1975, 94.

[51] Yusuf Ocak, Electrical characterization of DC sputtered ZnO/p-Si heterojunction, Journal of Alloys and Compounds 513, 2012, 130.

[52] Sedeek K., Said S.A., Amer T.Z., Makram N., Hantour H., Band gap tuning in nanocrystalline SrTi0.9 Fe0.1 O2.968 perovskite type for photocatalytic and photovoltaic applications. Ceram Int. 45(1), 2019, 1202.

[53] OJO, A. A. and Dharmadasa I.M., Progress in development of graded bandgap thin film solar cells with electroplated materials. Journal of Materials Science: Materials in Electronics, 28 (9), 2017, 6359.

[54] Wibowo A., Marsudi M.A., Amal M.I., Ananda M.B., Stephanie R., Ardy H. and Diguna L.J., ZnO nanostructured materials for emerging solar cell applications, RSC Adv 10, 2020, 42838.

[55] G.Sassi, Theoretical analysis of solar cells based on graded band-gap structures, J.Appl. Phys., 54, 1983, 5421.

[56] Alam A.E., Cranton W.M, Dharmadasa I.M., Electrodeposition of CdS thin-films from cadmium acetate and ammonium thiosulphate precursors, Journal of Materials Science: Materials in Electronics (2019) 30, 4580.

[57] Ahmed F., Lakhtakia A. and Monk P.B., Theory of graded - bandgap thin film solar cells, 2021, Morgan & Claypool publisher.

[58] An Q., Fabian Paulus F., Becker-Koch D., Cho C., Sun Q., Weu A., Bitton S., Tessler N. and Vaynzof Y., Small grains as recombination hot spots in perovskite solar cells, Matter, 2021, 1683.

[59] Fassl P., Ternes S., Lami V., Zakharko Y., Heimfarth D., Hopkinson P.E., Paulus F., Taylor A.D., Zaumseil J., and Vaynzof Y. Effect of crystal grain orientation on the rate of ionic transport in Perovskite polycrystalline thin films. ACS Appl. Mater. Interfaces, 11, 2019, 2490.

[60] Yang G., Tao H., Qin P., Ke W. and Fang G., Recent progress in electron transport layers for efficient perovskite solar cells, J. Mater. Chem. A, 4, 2016, 3970.

[61] Liu D. and Kelly T.L., Perovskite solar cells with a planar heterojunction structure prepared using room-temperature solution processing techniques, Nat. Photonics, 8, 2014, 133.

[62] Pandey R., Gupta S., Khatri T., Chaujar R., Interdigitated back contact silicon solar cell with perovskite layer for front surface passivation and ultraviolet radiation stability, 2017 IEEE 44th Photovoltaic Specialist Conference (PVSC).